Science of the Total Environment 655 (2019) 652–662

Contents lists available at ScienceDirect

Science of the Total Environment

journal homepage: www.elsevier.com/locate/scitotenv

The footprint of urban heat island effect in 302 Chinese cities: Temporal trends and associated factors

Qiquan Yang [a], Xin Huang [a,b,*], Qiuhong Tang [c,d,**]

[a] School of Remote Sensing and Information Engineering, Wuhan University, 129 Luoyu Road, Wuhan 430079, PR China
[b] State Key Laboratory of Information Engineering in Surveying, Mapping and Remote Sensing, Wuhan University, Wuhan 430079, PR China
[c] Key Laboratory of Water Cycle and Related Land Surface Processes, Institute of Geographic Sciences and Natural Resources Research, Chinese Academy of Sciences, Beijing 100101, PR China
[d] College of Resources and Environment, University of Chinese Academy of Sciences, Beijing 100049, PR China

HIGHLIGHTS

- The FP across China showed evident diurnal, seasonal and inter-city differences.
- The FP increased significantly in numerous Chinese cities during 2003–2016.
- The temporal variations of FP correlated to NL, EVI and WSA.
- More effective measures should be carried out to restrain the FP.

GRAPHICAL ABSTRACT

Temporal trends of the annual and seasonal (i.e. summer and winter) footprints of the surface urban heat island effect across 302 Chinese cities over the period 2003–2016.

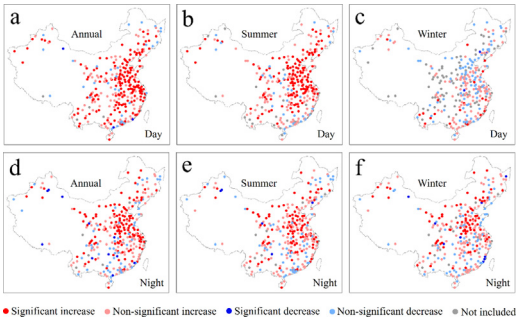

ARTICLE INFO

Article history:
Received 26 September 2018
Received in revised form 31 October 2018
Accepted 11 November 2018
Available online 12 November 2018

Editor: Ralf Ludwig

Keywords:
Urban heat island (UHI)
Land surface temperature (LST)
Temporal trend
Footprint
China

ABSTRACT

The urban heat island (UHI) effect has been a concern for decades due its adverse influence on energy consumption, air and water quality, and, most importantly, the health of urban dwellers. Researchers have paid much attention to the magnitude of the UHI effect, but ignored its spatial extent (i.e. footprint) which is another important aspect of the UHI effect. In this study, we systematically analyzed the footprint of surface UHI (SUHI) effect in 302 Chinese cities, especially temporal trends of the footprint, by using multi-source remote sensing data. The footprint of SUHI effect (FP) was estimated by the Gaussian surface, and its temporal trend was examined by the Mann-Kendal and the Sen's slope estimator non-parametric tests. We found the FP showed evident diurnal (daytime > nighttime), seasonal (summer > winter) and inter-city (big cities > small and medium-sized cities) differences. During the period 2003–2016, over 80% of the 302 cities exhibited increasing trends of the FP in annual days and summer days, and the increasing trends were statistically significant ($p < 0.05$) in about half of these cities. In the nights, the FP increased in more than 70% of the cities, and about one-third of the 302 cities experienced significantly increasing trends of the FP. On average, the annual daytime and annual nighttime FPs increased at a rate of 5.0% per year and 3.8% per year, respectively. More importantly, the correlation analysis indicated that the increase of anthropogenic heat emissions and the decrease of vegetation activities and surface albedos should take lead responsibility for the expansion of the FP in the urbanization

* Correspondence to: X. Huang, School of Remote Sensing and Information Engineering, Wuhan University, 129 Luoyu Road, Wuhan 430079, PR China.
** Correspondence to: Q. Tang, Key Laboratory of Water Cycle and Related Land Surface Processes, Institute of Geographic Sciences and Natural Resources Research, Chinese Academy of Sciences, Beijing 100101, PR China.
E-mail addresses: xhuang@whu.edu.cn, huang_whu@163.com (X. Huang), tangqh@igsnrr.ac.cn (Q. Tang).

https://doi.org/10.1016/j.scitotenv.2018.11.171

process. These results reveal that the spatial extent of heat island effect has expanded significantly in numerous Chinese cities, and this increasing trend will be sustained in the coming years if no more effective measures are carried out.

1. Introduction

The accelerating urbanization and the increasing anthropogenic activities have significantly modified the atmospheric and surface properties of the Earth, and have thus altered the energy balance in cities and affected the urban thermal environment (Grimm et al., 2008; Hart and Sailor, 2009; Yao et al., 2017). As a result, distinct temperature differences between urban areas and their less-developed surroundings have been widely observed, a phenomenon which has been termed the "urban heat island" (UHI) effect (Oke, 1982). The UHI effect is generally regarded as a result of the reduction in latent heat flux and the rise in sensible heat flux in urban areas (Imhoff et al., 2010). The UHI effect poses a threat to the air and water quality (Grimm et al., 2008; Rizwan et al., 2008), it greatly increases energy consumption in summer (Cui et al., 2017), and it results in increased thermal stress and heat health risk for urban dwellers (Dong et al., 2014; Vargo et al., 2016). Therefore, the UHI effect has been a concern for several decades (Oke, 1973; Oke, 1982).

Traditionally, air temperature monitored by in-situ stations has been widely applied to quantify the UHI effect (Atkinson, 2003; Ren et al., 2008). Although in-situ data have the advantage of stable and intensive time series, the limitation of the sparse spatial coverage makes such data unsuitable for identifying the spatial patterns of the UHI effect (Streutker, 2003). With the development of remote sensing techniques, land surface temperature (LST) data collected by satellites has been increasingly and widely used in the surface UHI (SUHI) studies due to its advantages of easier access, continuous coverage, and higher spatial resolution. Based on remote sensing data, we can not only obtain the magnitude of SUHI effect (SUHI intensity, SUHII), but also delineate the spatial extent of SUHI effect (referred as the footprint of SUHI effect in this study, FP).

The SUHII, which is defined as the surface temperature difference between urban and surrounding areas, is a popular indicator for the SUHI effect, and its spatial-temporal patterns have been discussed in majority of the SUHI studies (Cao et al., 2016; Imhoff et al., 2010; Liao et al., 2017; Peng et al., 2018; Peng et al., 2012; Yang et al., 2017; Yao et al., 2018; Zhang et al., 2014; Zhao et al., 2014; Zhou et al., 2017; Zhou et al., 2018; Zhou et al., 2016; Zhou et al., 2014). The FP is another important aspect of the SUHI effect, and it can give a picture of the spatial extent of the heat island effect. However, current researches on the FP are relatively scarce, and most of them are limited in single city. For example, Streutker (2002) firstly fitted the FP in Houston, Texas by using remote sensing data, and further analyzed its temporal variations (Streutker, 2003). Santamouris et al. (2007) found the SUHI in Athens, Greece could exert extensive influence on urban environment due to its large footprint. The obviously seasonal and diurnal variations of the FP were revealed both in Milan (Anniballe et al., 2014) and Shanghai (Sun et al., 2018). Considering the conclusions from single-city researches might be limited by local conditions, a few studies have attempted to investigate the FP in multiple cities. For instance, Tran et al. (2006) focused on the SUHI of eight Asian cities, and found the FP was highly positively correlated to the population size. Zhou et al. (2015) suggested large FPs in Chinese 32 major cities, and indicated their significant spatial heterogeneities. Unfortunately, there still exist some limitations in current multi-city investigations. Firstly, though spatial patterns of the FP have been detailed discussed, temporal trends of the FP and associated factors are still unclear. Secondly, researchers paid too much attention to large cities, but ignored lots of small and medium-sized cities. Therefore, a more comprehensive assessment of the FP, especially its temporal trend, is in need.

China has experienced rapid urban growth during recent decades, and the sustained urbanization has induced considerable variations in urban climates (Grimm et al., 2008). Consequently, the SUHI effect, especially its footprint, would have probably changed a lot with the urban development. Besides, the development level of cities in China varies greatly due to geographical, historical, and policy factors. There are not only big cities such as Beijing, but also a large number of medium and small cities across China, which provides a good chance to discover the different characteristics of the FP in cities with different development levels. Therefore, we conducted a comprehensive and detailed analysis of the FP in 302 Chinese cities. The main aims of this research were: 1) to give a picture of the spatial patterns of the FP across China; 2) to examine temporal trends of the FP in Chinese cities for the period of 2003–2016; and 3) to further investigate possible factors associated with temporal variations of the FP. Our analysis was based on multi-source datasets including the China's Land Use/Cover Datasets (CLUDs), the MODIS LST product and several other remote sensing products. The FP for each city was estimated by the Gaussian surface, and its temporal trend was examined by the Mann-Kendal (MK) and the Sen's slope estimator non-parametric tests.

2. Data and methods

2.1. Data

302 Chinese cities, including 4 municipalities, 27 provincial capitals, 264 prefecture-level cities, and 7 autonomous prefectures, were selected in this study (Fig. 1 and Supplementary Table S1). For each city, we extracted one study region (see Methods and Fig. 1) made up of the urban core area and its surrounding suburban area. All the cities were stratified by population size which was calculated by multiplying the size of the study region by the mean population density from the Gridded Population Database of China (http://www.resdc.cn). The cities were classified into three levels (Larkin et al., 2016): Level 1 (>1,000,000, population size), Level 2 (250000–1,000,000), and Level 3 (<250,000).

The study region of each city was extracted based on land-cover data and surface elevation data (Table 1). The land-cover data of each city were derived from the CLUDs (i.e. China's Land Use/Cover Datasets) provided by the Chinese Academy of Sciences. The CLUDs (30 m spatial resolution) were updated every five years from 1990 to 2015 using Landsat TM/ETM+ and HJ-1A/1B imagery. The original datasets contain 25 categories, and the overall accuracy of these datasets has been reported to be higher than 90% (Kuang et al., 2016; Liu et al., 2017). We reclassified the categories into six classes (built-up, cropland, vegetation, bare land, water, and other land) for further analysis. The surface elevation data were obtained from the Space Shuttle Radar and Topography Mission (SRTM), with a spatial resolution of approximately 90 m (SRTM90, Table 1).

LST, which is a prerequisite for quantifying the SUHI effect, was obtained from the EOS-Aqua-MODIS 8-day composite product (MYD11A2, Table 1) during the period of 2003–2016 for each city. The MYD11A2 data were acquired in both the daytime (13:30) and nighttime (01:30), with a spatial resolution of 1000 m. Wan (2008) reported that the accuracy of the MODIS LST data was better than 1 K, and the root-mean-square difference between the MODIS LST data and the in situ LST measurements was found to be <0.5 K across 39 tested cases. The advantages

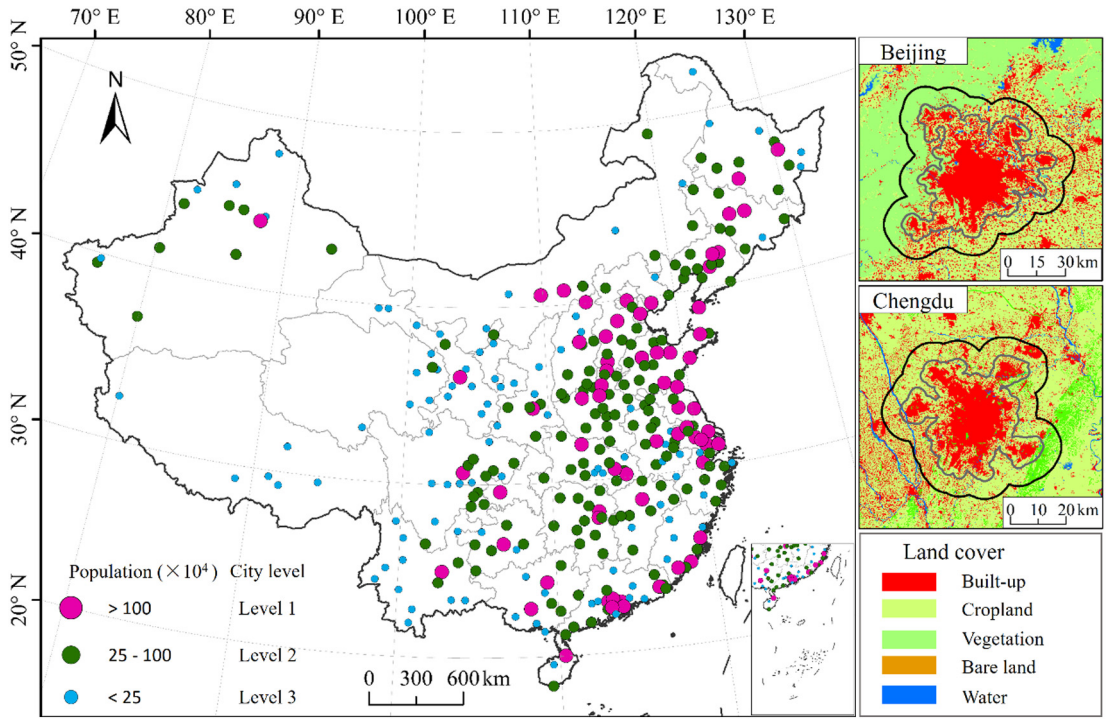

Fig. 1. Locations of the 302 Chinese cities, and examples of the delineation of study regions in Beijing and Chengdu. All the cities were classified into Level 1, Level 2 and Level 3 according to the population size. The land-cover maps on the right are based on China's Land Use/Cover Datasets (CLUDs) for 2010. The inner gray line and the outer black line in the land-cover maps represent the borders of the urban core area and the study region, respectively.

of the high temporal resolution, wide coverage, and high precision make the MODIS LST data ideal for exploring temporal trends of the FP.

To explore factors affecting temporal variations of the FP, we combined satellite observations of vegetation index, surface albedo, and anthropogenic heat release (Table 1). The MODIS monthly enhanced vegetation index (EVI) product (MYD13A3, 1000 m spatial resolution) was applied to indicate the vegetation activity for the period of 2003–2016, and the white sky albedo (WSA) information for 2003–2016 was extracted from the MODIS Bidirectional Reflectance Distribution Function (BRDF) albedo data (MCD43B3, 1000 m spatial resolution, and 8-day interval). According to previous studies (Liao et al., 2017; Peng et al., 2012), remotely sensed nighttime light (NL) data were an ideal proxy for anthropogenic heat release. Thus the DMSP/OLS stable NL product (version 4, 1000 m spatial resolution) after processing (Liu et al., 2012) of inter-calibration, intra-annual composition, and inter-annual correction was used to reflect the heat release by human activities.

2.2. Methods

2.2.1. Extraction of the study region

We focused on 302 Chinese cities in this study (Fig. 1). In each city, we extracted one study region which was defined as the composite of two parts: the urban core area and its equal-area surroundings. The extraction of the urban core area was based on the following three steps (Zhou et al., 2014): 1) generating a built-up intensity (i.e. BI) map for each city by the 1 km × 1 km moving window method based on the reclassified CLUD land-cover map; 2) separating the BI map into high- and low-intensity built-up land according to the 50% threshold of BI; and 3) aggregating the high-intensity built-up polygons by an aggregation distance of 2 km, where the land within the aggregation border was considered as the urban core area. The combination of the urban core area and its equal-area surroundings formed the study region of a city (Fig. 1). Note that, for each city, only one urban core area was included in the study region. Furthermore, to reduce bias, water pixels were removed from each study region, and pixels in the surrounding areas with topographic elevations ±50 m off the mean elevation of the urban core area were excluded from the study region of each city (Imhoff et al., 2010).

2.2.2. Calculation of the FP

To obtain the FP (i.e. the footprint of SUHI effect) for each city, a classical method proposed by Streutker (Streutker, 2003; Streutker, 2002) was used in this study. The overall idea of this method is that the spatially distributed heat island can be described by a two-dimensional Gaussian surface. This method has been widely used in UHI studies (Anniballe and Bonafoni, 2015; Anniballe et al., 2014; Keeratikasikorn and Bonafoni, 2018; Quan et al., 2014; Rajasekar and Weng, 2009; Tran et al., 2006) due to its good performance of the heat island modeling. Besides, the SUHI signal modeled by this method can give a

Table 1
Datasets used in this study.

Datasets (abbr.)	Resolution	Time	Usage
China's land use/cover datasets (CLUDs)	30 m	2005, 2010 and 2015	Mapping land cover and extracting study region of each city
MODIS LST product (MYD11A2)	1000 m	Every 8 days from 2003 to 2016	Providing LST data for quantifying the FP
Gridded population database of China	1000 m	2010	Stratifying cities into different levels
Surface elevation data (SRTM90)	90 m	/	Removing the influence of topographic relief
MODIS EVI product (MYD13A3)	1000 m	Each month from 2003 to 2016	Analyzing the relationship between the FP and associated factors (EVI, WSA and NL)
MODIS albedo product (MCD43B3)	1000 m	Every 8 days from 2003 to 2016	
DMSP/OLS stable NL product	1000 m	Each year from 2003 to 2013	

comprehensive representation of the urban thermal distribution (Quan et al., 2014), which makes this method an ideal tool to investigate the FP. The Gaussian surface used to fit the spatial distributed heat island can be described as follows:

$$T(x,y) = T_0 + a_1 x + a_2 y + a_0 \times \exp\left[-\frac{((x-x_0)\cos\varphi + (y-y_0)\sin\varphi)^2}{0.5{a_x}^2} - \frac{((y-y_0)\cos\varphi - (x-x_0)\sin\varphi)^2}{0.5{a_y}^2}\right]$$

where (x,y) represents the location of a pixel, $T(x,y)$ is the LST of a pixel at (x,y), T_0 is the background LST, a_1 and a_2 are regression coefficients for the planar surface of rural LST, φ is the orientation of the Gaussian surface, x_0 and y_0 reflect the central position, a_0 is the magnitude, and a_x and a_y are the half long and short axes of the Gaussian bottom ellipse, respectively.

The parameters in the equation were estimated by the following steps. Firstly, in the study region of a city, the LST pixels belonging to the urban area (i.e. built-up area) were temporarily masked out, generating an LST map consisting entirely of rural pixels. Secondly, the rural LST parameters (T_0, a_1, and a_2 in the equation) were estimated for all the remaining LST pixels using linear regression. Finally, the planar surface of rural LST was subtracted from the $T(x,y)$ image, and the resulting LST was fitted to the Gaussian surface. The FP can be expressed by the area of the ellipse that cross the Gaussian surface at which the temperature is higher than 1 K (Anniballe et al., 2014; Streutker, 2003). All the analysis was based on the nls (nonlinear least squares) function which is an effective tool to estimate parameters of a nonlinear model in the R stats package. In addition, it is noticeable that data concurrency is necessary when estimating the SUHI effect (Zhao et al., 2016). Thus, the land cover maps extracted from CLUDs in 2005, 2010 and 2015 were used to estimate the FPs during the period 2003–2007, 2008–2012 and 2013–2016, respectively.

For each city, both the daytime and nighttime FPs were fitted by the Gaussian surface every 8 days from 2003 to 2016 using the MODIS LST product. To improve the reliability of the results, the fitted FPs meeting any of the following conditions were removed: 1) the valid pixels in the LST image cover <50% of the study region; 2) the correlation coefficient between the surface temperature and the SUHI signal modeled by the Gaussian surface is <0.5 (Quan et al., 2014); and 3) the FP is out of the 99% confidence interval in the time series. The remaining fitted FPs after the above data filtering were used for the further analysis.

2.2.3. Temporal trend analysis of the FP

The MK (i.e. Mann-Kendal) and the Sen's slope estimator non-parametric tests were applied in this study to examine the temporal trends of the FP during 2003–2016. These methods have been widely applied in the trend analysis of climatic and environmental variables (Karabulut et al., 2008; Mondal et al., 2015; Thompson and Paull, 2017), because of the fact that they do not require any hypotheses about the variables and they are more powerful than parametric tests for short time series (Fernandes and Leblanc, 2005; Planque et al., 2017).The MK test was used to decide if a significant trend of the FP happened. The null hypothesis (H_0) of the MK test assumes that the data are independent and randomly ordered, i.e., there is no significant trend. In a two-tailed t-test, if the significance level was below than 0.05, the null hypothesis was rejected, and a significant temporal trend of the FP was detected. Besides, the change tendency (increase or decrease) was indicated by the sign of the Sen's slope. Therefore, the temporal tendencies of the FP for cities across China include four types: significantly ($p < 0.05$, the MK test) increasing trend (SIT), non-significantly increasing trend (NSIT), significantly decreasing trend (SDT), and non-significantly decreasing trend (NSDT). Besides, for cities with significant trends of the FP, we could obtain the change rate of the FP (FP_{CR}) by the Sen's slope. The FP_{CR} is robust to outliers because that the Sen's slope calculates the median slope rather than the mean slope extracted by parametric liner regressions. The MK and Sen's slope estimator non-parametric tests were implemented by the mannKen function in the R wql package.

Due to the obvious seasonal variations of the heat island effect (Peng et al., 2012), both annual and seasonal (summer: from June to August, and winter: from December to February) trends of the FP were analyzed. For each city, we firstly calculated annually and seasonally average FPs for each year during 2003–2016, and then analyzed the temporal trends of the FP across years. Furthermore, to further ensure that the results of the trend analysis were robust, only cities with at least 10 years of available FP values were included. As a result, cities finally included in the trend analysis were part of the initial 302 cities (Table 2).

2.2.4. Factors associated with temporal variations of the FP

To explore possible factors affecting temporal variations of the FP, we conducted correlation analysis between the FP and three variables (nighttime light (NL), enhanced vegetation index (EVI), and white sky albedo (WSA)) across years in each city. These variables are able to comprehensively reflect various aspects of cities and have been used in numerous studies related to heat island effect (Du et al., 2016; Peng et al., 2012; Zhou et al., 2014). In the study region for each city, we calculated mean values of the EVI and the WSA for every image during 2003–2016, and then annually and seasonally averaged them in each year. However, the NL was only annually averaged in each year during 2003–2013, as the DMSP/OLS stable NL product was annually compiled (without seasonal information) database available until 2013. In addition, for each city, the images of these variables with too many missing pixels (>50% of the study region) were removed from our analysis. The FP and the above-mentioned variables (NL, EVI and WSA) were arranged in pairs by year for each city, and then the Spearman's correlation analysis, a non-parametric method, was applied to assess the relationship between the FP and these variables across years. The significance test was performed by a two-tailed t-test, and the standard 0.05 significance level was adopted. Besides, the Spearman's correlation analysis might be no functioning in some cities due to the insufficient number of paired values, and these cities would be labeled as “Failed”. All the correlation analyses were finished by the cor function in the R Stats package.

3. Results

3.1. Spatial patterns of the FP

Fig. 2 shows the spatial patterns of the FP averaged over the period 2003–2016 for Chinese 302 cities and the mean FPs of different levels of city. The FP varied greatly among cities, from 10.8 km^2 (Shigatse) to 3738.6 km^2 (Shenzhen) in annual days (Fig. 2a) and from 4.16 km^2 (Hechi) to 830.6 km^2 (Beijing) in annual nights (Fig. 2b). Overall, the annual daytime and annual nighttime mean FPs for all cities were 151.5 [106.7, 196.2] (values in parenthesis define the 95% confidence interval, hereafter) km^2 (Fig. 2c) and 61.3 [50.9, 71.6] km^2 (Fig. 2d), respectively.

Table 2
The number of cities included in the trend analysis (the Mann-Kendal and Sen's slope estimator tests) during the different seasons and different city levels. Some cities were not included in the trend analysis because there were <10 valid FP values.

City level	The number of all cites	The number of cities included in the trend analysis					
		Daytime			Nighttime		
		Annual	Summer	Winter	Annual	Summer	Winter
Level 1	65	65	62	60	65	64	64
Level 2	155	155	153	123	155	154	154
Level 3	82	78	67	41	76	74	66
All cities	302	298	282	224	296	292	284

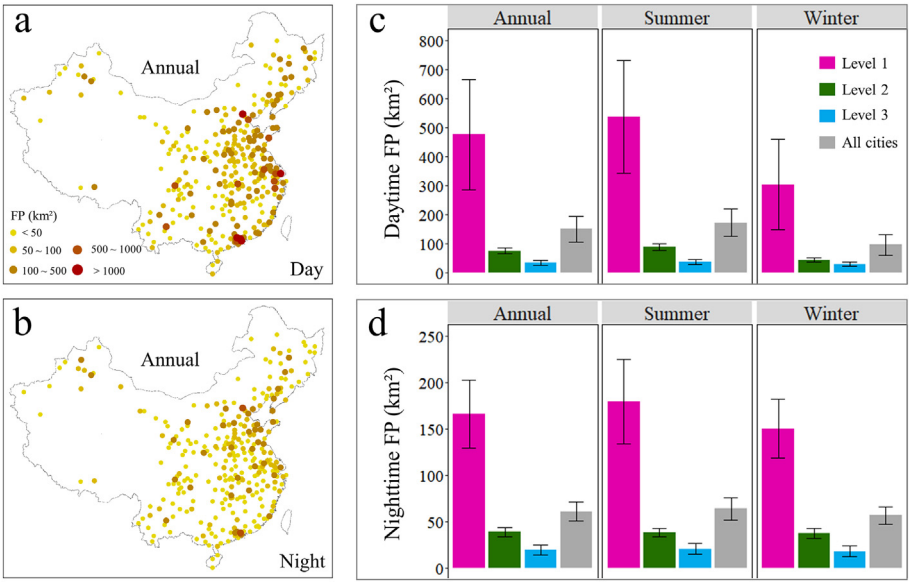

Fig. 2. The spatial distribution of the annual (a) daytime and (b) nighttime FPs across 302 Chinese cities, and the mean FPs of different levels of city during the (c) day and (d) night. The vertical bars across the columns indicate the 95% confidence intervals of the FP.

Large cities tend to experience larger FPs than small cities. For instance, the annual mean FPs were in a descending order of Level 1 > Level 2 > Level 3 at both daytime (477.0 vs. 76.3 vs. 35.5 km^2, $p < 0.001$) and nighttime (166.2 vs. 39.2 vs. 19.8 km^2, $p < 0.001$), and this phenomenon was also observed in summer and winter (Fig. 2). Besides, the daytime FPs were generally lager in the summer than the winter period (172.5 vs. 97.3 km^2, $p < 0.01$) (Fig. 2c), whereas the nighttime FPs were similar in both seasons (64.2 vs. 56.9 km^2, $p = 0.339$) (Fig. 2d).

3.2. Temporal trends of the FP

The temporal trends of the FP across all cities are demonstrated in Fig. 3, and their corresponding statistical results are shown in Figs. 4–5. In annual days and summer days, the increasing trends of the FP were observed in over 80% of the 302 cities, and the increasing trends were statistically significant ($p < 0.05$) in about half of these cities (167 of 302 for annual days, 143 of 302 for summer days) (Figs. 4–5). In the nights, the FP increased in more than 70% of the 302 cities, and about one-third of the 302 cities experienced significantly increasing trends of the FP (Figs. 4–5). The number of cities with a SIT (i.e. significantly increasing trend) of the FP was much greater in summer days than that in winter days (143 vs. 20), but this seasonal difference was much smaller at nights (97 vs. 80) (Fig. 4). The percentage of cities with a SIT of the FP in bigger cities was generally higher than that in smaller cities, especially in summer days (60.0% (Level 1) vs. 51.0% (Level 2) vs. 30.5% (Level 3)) (Fig. 5). Besides, few cities showed a SDT (i.e. significantly decreasing trend) of the FP during both daytime (no city for summer, and 3 cities for winter) and nighttime (5 cities for summer, and 9 cities for winter) (Fig. 4).

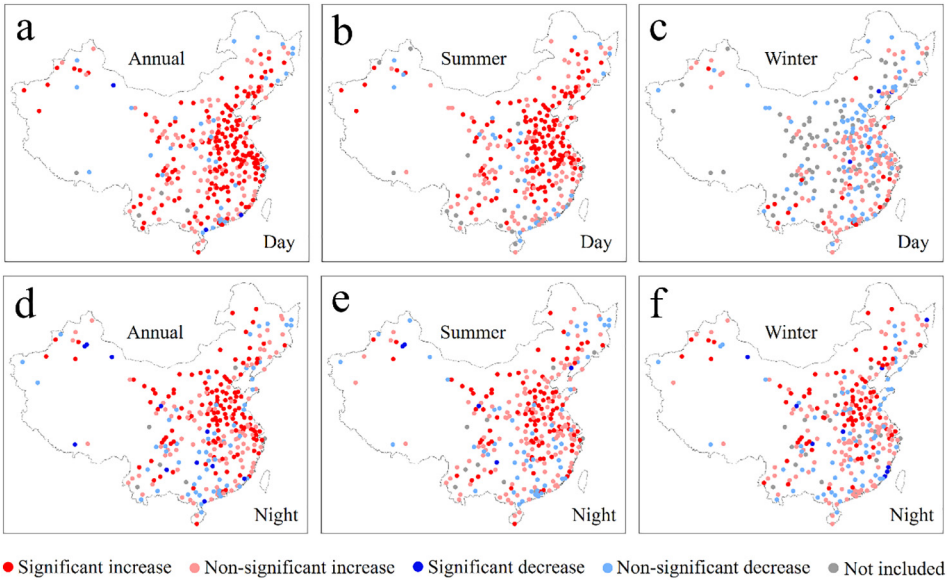

Fig. 3. The temporal trends of the annual and seasonal (i.e. summer and winter) FPs across 302 China's cities over the period 2003–2016. The upper rows (a, b, and c) are the daytime results, and the lower rows (d, e, and f) are the nighttime results. Some cities not included in the trend analysis were labeled as "Not included" in the figures.

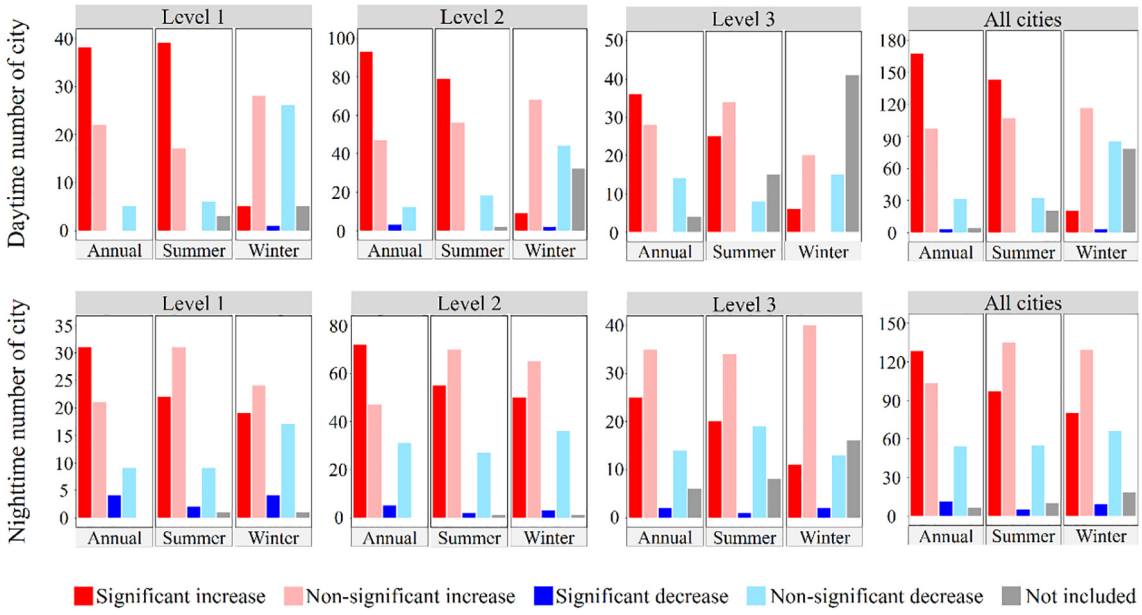

Fig. 4. The number of cities with different types of the temporal trends of the FP. The upper rows are the daytime results, and the lower rows are the nighttime results. "Not included" in the legend represents some cities not included in the trend analysis.

3.3. Change rates of the FP

Due to the rareness of cities with a SDT of the FP (Figs. 3–5), we would only focused on the FP_{CR} (i.e. change rate of the FP) of cities with a SIT of the FP. The FP_{CR} varied greatly among cities, and grew linearly with the FP (Fig. 6). Similar to the FP, the FP_{CR} also showed obvious difference among cities at different levels (Level 1 > Level 2 > Level 3, $p < 0.001$), and differed significantly among seasons (summer > winter, $p < 0.01$) (Fig. 6). For all the cities with a SIT of the FP, the FP_{CR} was 6.2 [4.8, 7.6] km^2/year in annual days, and 2.7 [1.9, 3.5] km^2/year in annual nights during the period 2003–2016 (Fig. 6).

In addition to absolute values of the FP_{CR}, we paid more attention to the relative rate of the FP (i.e. relative FP_{CR}). The relative FP_{CR} was defined as the ratio of FP_{CR} to FP because of the positive relation between the FP_{CR} and FP (Fig. 6). Overall, the relative FP_{CR} was 5.0% [4.7%, 5.3%] per year in annual days, and 3.8% [3.4%, 4.1%] per year in annual nights (Fig. 7). However, the seasonal difference in the relative FP_{CR} was not significant during both daytime (summer: 5.7% vs. winter: 6.8%, $p = 0.068$) and nighttime (summer: 4.9% vs. winter: 4.5%, $p = 0.145$) (Fig. 7). Besides, there was no significant difference in the relative FP_{CR} among cities at different levels ($p > 0.05$).

3.4. Factors associated with temporal variations of the FP

The FP correlated positively with the NL in most cities (Fig. 8 and Supplementary Fig. S1–2). Positive correlations between the FP and the NL were found in over 90% of the cities in annual days (283 of 302, Table 3) and summer days (278 of 302, Supplementary Table S2), and more than 80% of the cities in the nighttime (Table 3 and Supplementary Table S2–3). More importantly, the positive correlations between the FP and the NL were statistically significant in about one-third cities in both annual daytime (131 of 302, Table 3) and summer daytime (103 of 302, Supplementary Table S2). These indicated the increasing NL would probably contribute to the enlarging of the FP.

In contrast, the FP was negatively correlated to the EVI and WSA in a large number of cities (Fig. 8 and Supplementary Fig. S1–2). Negative correlations between the FP and the EVI were observed in about 80% of the cities in summer (235 of 302 at daytime, and 264 of 302 at nights,

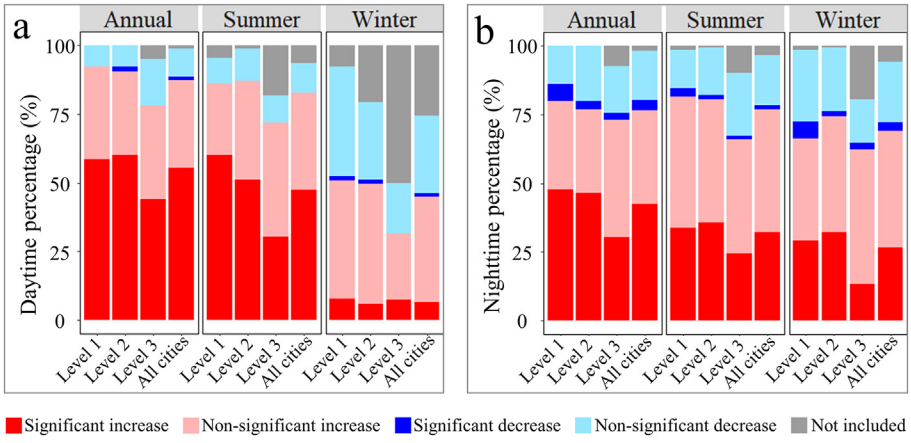

Fig. 5. The percentage of cities with different types of the temporal trends of the FP during the (a) daytime and (b) nighttime. "Not included" in the legend represents some cities not included in the trend analysis.

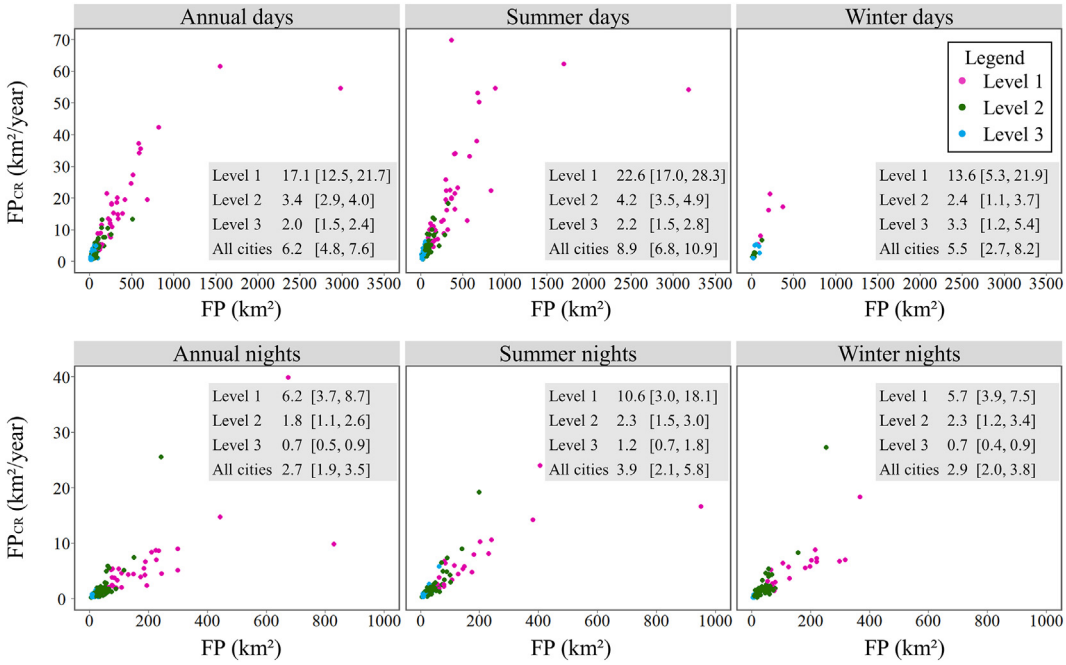

Fig. 6. The scatter plots of the annual and seasonal (summer and winter) FP_{CR} against the FP. The mean FP_{CR} (with 95% confidence intervals in parenthesis) of cities at different levels are listed in the gray panel of each plot. The upper rows are the daytime results, and the lower rows are the nighttime results.

Supplementary Table S2), while about 60% of the cities in winter (193 of 302 for both daytime and nighttime, Supplementary Table S3). Meanwhile, the FP correlated negatively to the WSA in about 70% cities in annual daytime (222 of 302) and annual nighttime (209 of 302) (Table 3). However, only a small part of these negative correlations were statistically significant (Table 3 and Supplementary Table S2–3).

4. Discussion

4.1. Extensively expanding FPs across Chinese cities

The spatial patterns and temporal trends of the FP across 302 Chinese cities were systematically analyzed. Our findings corroborated the extensive FPs in numerous Chinese big cities as revealed in previous researches (Tran et al., 2006; Zhou et al., 2015). For instance, the annual daytime FP reached up to 3738.6 km^2 in Shenzhen and 2985.1 km^2 in Beijing (Fig. 2). Besides, considerable FPs were also observed in several medium and small cities such as Jinhua (510.5 km^2) and Shaoguan (275.0 km^2) (Fig. 2). The large extent of the FP would no doubt cause heat stress to large amount of urban dwellers, especially during hot summer. We estimated the number of people suffered from the SUHI effect by calculating the population within the footprint of the SUHI effect across 302 cities according to the Gridded Population Database of China (http://www.resdc.cn). The results indicated that during the period 2003–2016, the daytime and nighttime SUHI effect influenced over 100 million people and about 50 million people, respectively, each year (Fig. 9). Note that these were merely the total population affected by the SUHI effect in these 302 Chinese cities, and in fact there shall be much more people enveloped by the heat island effect across China. To alleviate the influence of the SUHI effect, it is necessary to reduce the spatial extent of the heat island effect.

Unfortunately, we found the FP showed a significantly increasing trend in a large number of cities during the past decade. The annual daytime FP increased significantly in about half of the 302 cities (Fig. 5), with a relative increasing rate of 5.0% [4.7%, 5.3%] per year (Fig. 7). In the annual nighttime, the FP increased significantly in approximately

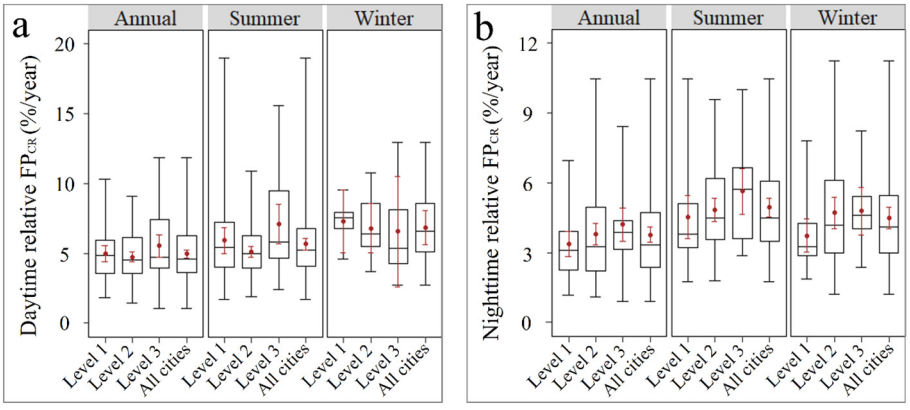

Fig. 7. The boxplots of the annual and seasonal (summer and winter) relative FP_{CR} during (a) daytime and (b) nighttime. The relative FP_{CR} is equal to the ratio of FP_{CR} to FP. The boxes represent the 25th and 75th percentiles, with the whiskers extend to the minimum and maximum values. The horizontal black lines inside the boxes are the medians. The red points represent the mean values, and the red line segments represent the 95% confidence intervals around them. (For interpretation of the references to colour in this figure legend, the reader is referred to the web version of this article.)

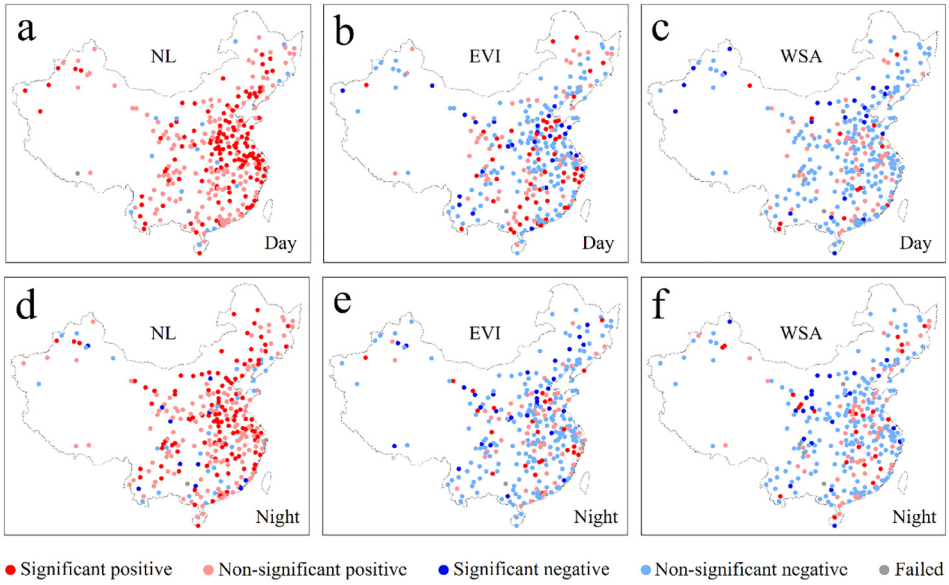

Fig. 8. Spearman's correlation analysis between the annual daytime and annual nighttime FPs and the nighttime light (NL), the vegetation index (EVI), and the white sky albedo (WSA) across years. The significance test was performed by a two-tailed *t*-test, and the standard 0.05 significance level was adopted. The "Failed" in the legend represents cities that failed in the correlation analysis.

one-third of the 302 cities (Fig. 5), and the average relative increasing rate was 3.8% [3.4%, 4.1%] per year (Fig. 7). In contrast, few cities showed a significantly decreasing trend of the FP (Fig. 5). The significant increase of the FP would further expand the influence of the SUHI effect. According to the results of trend analysis, we could clearly find that the total population suffered from the SUHI effect has increased significantly ($p < 0.01$) in all seasons (except for winter days) from 2003 to 2016 (Fig. 9). This means that more people might be influenced by the heat island effect in the coming years as the rapid urbanization in China would be sustained. More importantly, as the population enveloped by heat island effect grows, energy consumption by human activities will also increase, especially during hot summer when people need more electric power for air-conditioning cooling, which will in turn deteriorate the heat island effect. Therefore, it is indeed necessary for us to decrease the FP or at least restrain the expansion of the FP.

Table 3
Statistical results of the Spearman's correlation analysis between the annual daytime and annual nighttime FPs and the nighttime light (NL), the vegetation index (EVI), and the white sky albedo (WSA). Both the number and percentage of cities with different types of the correlation were represented in the following table. The types of the correlation including significant positive correlation, non-significant positive correlation, significant negative correlation, and non-significant negative correlation. The significance test was performed by a two-tailed t-test, and the standard 0.05 significance level was adopted. Cities that failed in the correlation analyses were labeled as "Failed".

	NL		EVI		WSA	
	Days	Nights	Days	Nights	Days	Nights
Positive						
Significant	131 (43.4%)	114 (37.7%)	52 (17.2%)	24 (7.9%)	12 (4.0%)	24 (7.9%)
Non-significant	152 (50.3%)	145 (48.1%)	66 (21.9%)	61 (20.2%)	62 (20.5%)	65 (21.6%)
Negative						
Significant	0 (0%)	11 (3.6%)	26 (8.6%)	31 (10.3%)	21 (7.6%)	22 (7.3%)
Non-significant	17 (5.6%)	30 (9.9%)	157 (52.0%)	185 (61.3%)	201 (66.6%)	187 (61.9%)
Failed	2 (0.7%)	2 (0.7%)	1 (0.3%)	1 (0.3%)	4 (1.3%)	4 (1.3%)

4.2. Factors associated with the temporal variations of the FP

As revealed by the correlation analysis, the FP generally correlated positively to the NL, and negatively to the EVI and WSA (Fig. 8 and Supplementary Fig. S1–2). The NL is able to indicate the heat released by human activities in cities, the positive correlation between the FP and the NL signified more anthropogenic activities would probably induce larger spatial extend of the heat island effect. The EVI can reflect vegetation activities in cities, thus the FP was negatively correlated to the EVI as the presence of vegetation has a cooling effect on the surface temperature via transpiration (Peng et al., 2012). Materials with high albedo attain lower temperatures when exposed to solar radiation (Prado and Ferreira, 2005), this might be the reason for the negative relation between the WSA (an index of albedo) and the FP.

Rapid urbanization in China has largely modified the land cover and aggregated more people in urban areas. As a direct consequence of urbanization, the replacement of natural vegetation with man-made impervious surface resulted in the weakening of vegetation cooling effect and the decreasing of surface albedo (Zhou et al., 2014). Besides, the aggregation of urban dwellers increased more anthropogenic heat emissions in cities. In addition to the factors discussed in this research, the expansion of the SUHI effect could be related with several other phenomena during the rapid urbanization process. For instance, Zhou et al. (2017) found that the UHI effect was closely related with city size and urban form, which was supported by Sobstyl et al. (2018) and Bonafoni et al. (2017). Conclusions from Du et al. (2016) and Yao et al. (2018) suggested that climate condition variations played an important role in the heat island change. Besides, the deterioration of air pollution (Cao et al., 2016) and increase of population density (Zhou et al., 2018) were also driving factors of the heat island effect. Overall, the combination of these factors has led to the expansion of the heat island extent.

More attentions should be paid to the mitigation action of the heat island effect as the urbanization is expected to sustain in future decades (Seto et al., 2012). For restraining the spatial expansion of the heat island effect, we recommend several measures to urban planners and government officials. Firstly, increasing the coverage of plants in urban areas and protecting the existing urban green space, such as urban parks, are the most direct mitigation measures due to vegetation cooling

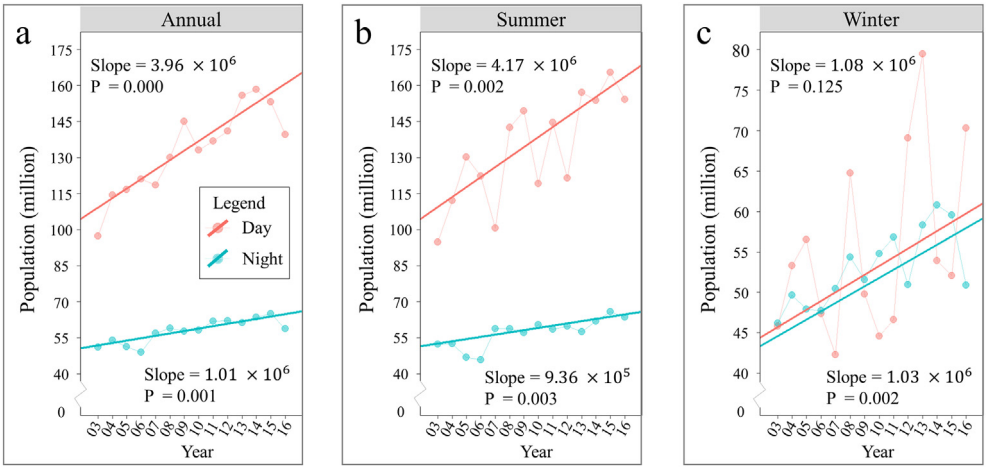

Fig. 9. The temporal trends of the total population affected by the (a) annual, (b) summer and (c) winter SUHI across 302 Chinese cities over the period 2003–2016. The population information was extracted from the Gridded Population Database of China (http://www.resdc.cn), and the trend analysis was based on the Mann-Kendal and Sen's slope estimator tests.

effect. Secondly, increasing urban surface albedo via adopting solar-reflective materials and landscape configuration is an effective way to relieve the heat island effect, which has been empirically verified (Mackey et al., 2012). Finally, the most important way is to reduce anthropogenic heat emissions by several measures including promoting energy-saving consciousness, improving energy consumption efficiency and advocating for public transportation.

4.3. Uncertainties

Some uncertainties in the present study need to be addressed. Firstly, only cities with at least ten-year available FPs were included in the trend analysis for ensuring the robustness. Most of the cities excluded from the trend analysis were small hilly cities located in the west of China (Fig. 3). The missing of LST data in these cities was very serious, which should take lead responsibility for the absence of the trend analysis. Besides, the FP in this study was fitted by the Gaussian surface. The performance of the fitting was assessed by the correlation coefficient between the initial LST and the fitted signals, and the results of poor fittings ($r < 0.5$) were excluded. The Gaussian surface performed very well in all cities except several small cities, and this is part of the reason that some cities were not included in the trend analysis. Therefore, future studies need to pay more attention to the LST data quality and the performance of the Gaussian surface when estimating the spatial extent of the SUHI effect.

Secondly, as we stated, the footprint of SUHI effect was fitted by the Gaussian surface. However, the associated factors (NL, EVI and WSA) were averaged in the study region of each city rather than fitted by the Gaussian surface. This is mainly due to following reasons. 1) The DMSP/OLS stable NL product was annually compiled database, and it means that only one Gaussian fitting surface can be obtained per year. This would induce insufficient number of available fitted NLs if the fitting effect is poor in several years. 2) The Gaussian assumption does not always apply to the vegetation and albedo data, which has also been revealed in a previous study (Quan et al., 2014). Therefore, as an alternative strategy, average values of these factors (NL, EVI and WSA) were used in this study. This strategy was thought to be reasonable because that the change of the footprint of these factors shall be much related to the variation of their average values. As expected, the FP correlated positively to the NL, and negatively to the EVI and WSA in most cities (Fig. 8). However, we should note that the conceptions of the footprint and the average value were not completely consistent, which would probably cause uncertainties to our results, e.g. positive relationship between the FP and the EVI and WSA in a few cities.

Thirdly, in several previous studies, the land cover was assumed constant and the analysis of the temporal trend of SUHI effect was based on a static land cover map (Peng et al., 2018; Zhou et al., 2016). However, the land cover was in deed changeable over time, especially in Chinese cities with rapid urbanization over past years. Therefore, in this study, dynamic land cover maps (2005, 2010 and 2015) were used when estimating the FPs during the period 2003–2016. To assess the uncertainties caused by the difference of using dynamic and static land cover maps, we conducted a comparison experiment. In the comparison experiment, we replaced the dynamic land cover maps with a static one (CLUD in the year of 2010), and kept the other experimental data and steps were exactly the same. The results of the comparison experiment corroborated the FP increased significantly in a large percentage of cities (Fig. 10). Besides, conclusion that few cities showed a significantly decreasing trend of the FP was also supported by the comparison experiment (Fig. 10). Moreover, the FP_{CR} of the two experiments were highly ($r > 0.9$ for most cases) and significantly ($p < 0.01$) correlated (Supplementary Table S4). Though the results of the two experiments were generally consistent, there were still some differences need to be noticed. For instance, the number of cities showed a SIT of the daytime FPs based on the static land cover map was smaller than that based on the dynamic land cover maps (136 vs. 167 in annual days, and 111 vs. 143 in summer days). This stressed the necessity of dynamic land cover maps when conducting trend analysis of the SUHI effect in Chinese cities with rapid urbanization.

5. Conclusion

In this study, we systematically analyzed temporal trends of the FP (i.e. the footprint of SUHI effect) across 302 Chinese cities during the period 2003–2016, using multi-source remote sensing data. The FP was estimated by the Gaussian surface, and its temporal trend was examined by the MK and the Sen's slope estimator non-parametric tests. The Spearman's correlation analysis was used to investigate the possible factors associated with temporal variations of the FP.

The FP varied greatly among cities, and big cities tended to have larger FPs than small and medium-sized cities. Besides, daytime FP was generally larger than nighttime FP, and the FP in summer was usually bigger than that in winter. Most cities (over 80%) experienced increasing trends of the FP in annual days and summer days, and the increasing trends were statistically significant ($p < 0.05$) in about half of these cities (167 of 302 for annual days, 143 of 302 for summer days). In the nights, the FP increased in more than 70% of the 302 cities, and about one-third of these cities experienced significantly increasing trends of the FP. Similar to the FP, the change rate of the FP (i.e. FP_{CR})

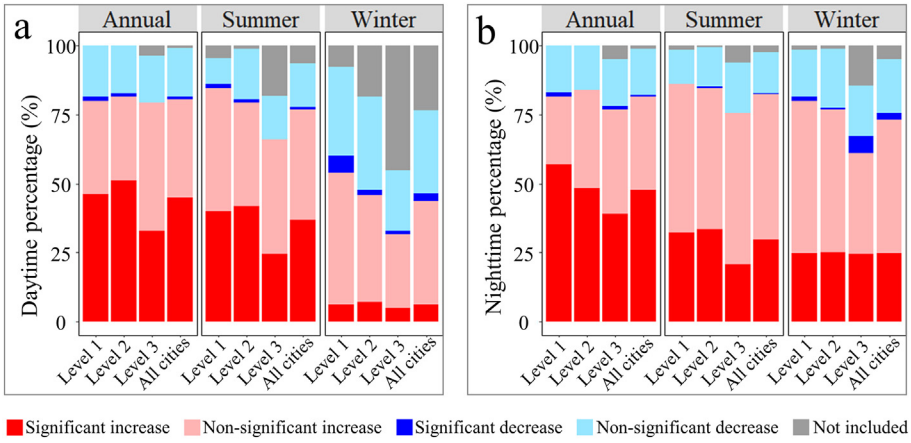

Fig. 10. The percentage of cities with different types of the temporal trends of the FP during the (a) daytime and (b) nighttime based on a static land cover map (CLUDs in the year of 2010). "Not included" in the legend represents some cities not included in the trend analysis.

also showed evident diurnal (daytime > nighttime), seasonal (summer > winter) and inter-city (big cities > small and medium-sized cities) differences. However, the relative FP_{CR}, defined as the ratio of FP_{CR} to FP, seemed to be similar between seasons and cities at different levels. On average, the FP increased at a rate of 5.0% per year and 3.8% per year in annual days and annual nights, respectively, from 2003 to 2016. Importantly, we found that the FP was positively correlated to the NL, and negatively correlated to the EVI and WSA for most cities, which indicated that the increase of anthropogenic heat emissions and the decrease of vegetation activities and surface albedos in the process of urbanization should take lead responsibility for the expansion of the FP.

In summary, Chinese cities are experiencing extensive heat island effect, and the spatial extent of the heat island effect is expected to be expanding in the coming years. Therefore, urban planners and government officers must be serious about this and take more effective measures to prevent the deterioration of our living environment.

Acknowledgments

This research was supported by the National Natural Science Foundation of China under grants 41522110, 41771360, and 41790424; the Hubei Provincial Natural Science Foundation of China under Grant 2017CFA029; and the National Key Research and Development Program of China under Grant 2016YFB0501403.

Appendix A. Supplementary data

Supplementary data to this article can be found online at https://doi.org/10.1016/j.scitotenv.2018.11.171.

References

Anniballe, R., Bonafoni, S., 2015. A stable Gaussian fitting procedure for the parameterization of remote sensed thermal images. Algorithms 8, 82–91.
Anniballe, R., Bonafoni, S., Pichierri, M., 2014. Spatial and temporal trends of the surface and air heat island over Milan using MODIS data. Remote Sens. Environ. 150, 163–171.
Atkinson, B.W., 2003. Numerical modelling of urban Heat-Island intensity. Bound.-Layer Meteorol. 109, 285–310.
Bonafoni, S., Baldinelli, G., Verducci, P., Presciutti, A., 2017. Remote sensing techniques for urban heating analysis: a case study of sustainable construction at district level. Sustainability 9.
Cao, C., Lee, X., Liu, S., Schultz, N., Xiao, W., Zhang, M., et al., 2016. Urban heat islands in China enhanced by haze pollution. Nat. Commun. 7, 12509.
Cui, Y., Yan, D., Hong, T., Ma, J., 2017. Temporal and spatial characteristics of the urban heat island in Beijing and the impact on building design and energy performance. Energy 130, 286–297.
Dong, W., Liu, Z., Zhang, L., Tang, Q., Liao, H., Li, X.E., 2014. Assessing heat health risk for sustainability in Beijing's urban heat island. Sustain. For. 6, 7334–7357.
Du, H., Wang, D., Wang, Y., Zhao, X., Qin, F., Jiang, H., et al., 2016. Influences of land cover types, meteorological conditions, anthropogenic heat and urban area on surface urban heat island in the Yangtze River Delta urban agglomeration. Sci. Total Environ. 571, 461–470.
Fernandes, R., Leblanc, S.G., 2005. Parametric (modified least squares) and non-parametric (Theil-Sen) linear regressions for predicting biophysical parameters in the presence of measurement errors. Remote Sens. Environ. 95, 303–316.
Grimm, N.B., Faeth, S.H., Golubiewski, N.E., Redman, C.L., Wu, J., Bai, X., et al., 2008. Global change and the ecology of cities. Science 319, 756–760.
Hart, M.A., Sailor, D.J., 2009. Quantifying the influence of land-use and surface characteristics on spatial variability in the urban heat island. Theor. Appl. Climatol. 95, 397–406.
Imhoff, M.L., Zhang, P., Wolfe, R.E., Bounoua, L., 2010. Remote sensing of the urban heat island effect across biomes in the continental USA. Remote Sens. Environ. 114, 504–513.
Karabulut, M., Gürbüz, M., Korkmaz, H., 2008. Precipitation and temperature trend analyses in Samsun. J. Int. Environ. Appl. Sci. 3, 399–408.
Keeratikasikorn, C., Bonafoni, S., 2018. Satellite images and Gaussian parameterization for an extensive analysis of urban heat islands in Thailand. Remote Sens. 10, 665.
Kuang, W., Liu, J., Dong, J., Chi, W., Zhang, C., 2016. The rapid and massive urban and industrial land expansions in China between 1990 and 2010: a CLUD-based analysis of their trajectories, patterns, and drivers. Landsc. Urban Plan. 145, 21–33.
Larkin, A., van Donkelaar, A., Geddes, J.A., Martin, R.V., Hystad, P., 2016. Relationships between changes in urban characteristics and air quality in East Asia from 2000 to 2010. Environ. Sci. Technol. 50, 9142–9149.
Liao, W., Liu, X., Wang, D., Sheng, Y., 2017. The impact of energy consumption on the surface urban heat island in China's 32 major cities. Remote Sens. 9, 250–262.
Liu, Z., He, C., Zhang, Q., Huang, Q., Yang, Y., 2012. Extracting the dynamics of urban expansion in China using DMSP-OLS nighttime light data from 1992 to 2008. Landsc. Urban Plan. 106, 62–72.
Liu, W., Liu, J., Kuang, W., Ning, J., 2017. Examining the influence of the implementation of major function-oriented zones on built-up area expansion in China. J. Geogr. Sci. 27, 643–660.
Mackey, C.W., Lee, X., Smith, R.B., 2012. Remotely sensing the cooling effects of city scale efforts to reduce urban heat island. Build. Environ. 49, 348–358.
Mondal, A., Khare, D., Kundu, S., 2015. Spatial and temporal analysis of rainfall and temperature trend of India. Theor. Appl. Climatol. 122, 143–158.
Oke, T.R., 1973. City size and the urban heat island. Atmos. Environ. 7, 769–779.
Oke, T.R., 1982. The energetic basis of the urban heat island. Q. J. R. Meteorol. Soc. 108, 1–24.
Peng, S., Piao, S., Ciais, P., Friedlingstein, P., Ottle, C., Breon, F.M., et al., 2012. Surface urban heat island across 419 global big cities. Environ. Sci. Technol. 46, 696–703.
Peng, J., Ma, J., Liu, Q., Liu, Y., Li, Y., Yue, Y., 2018. Spatial-temporal change of land surface temperature across 285 cities in China: an urban-rural contrast perspective. Sci. Total Environ. 635, 487–497.
Planque, C., Carrer, D., Roujean, J.-L., 2017. Analysis of MODIS albedo changes over steady woody covers in France during the period of 2001–2013. Remote Sens. Environ. 191, 13–29.
Prado, R.T.A., Ferreira, F.L., 2005. Measurement of albedo and analysis of its influence the surface temperature of building roof materials. Energy Build. 37, 295–300.
Quan, J., Chen, Y., Zhan, W., Wang, J., Voogt, J., Wang, M., 2014. Multi-temporal trajectory of the urban heat island centroid in Beijing, China based on a Gaussian volume model. Remote Sens. Environ. 149, 33–46.
Rajasekar, U., Weng, Q., 2009. Spatio-temporal modelling and analysis of urban heat islands by using Landsat TM and ETM+ imagery. Int. J. Remote Sens. 30, 3531–3548.
Ren, G., Zhou, Y., Chu, Z., Zhou, J., Zhang, A., Guo, J., et al., 2008. Urbanization effects on observed surface air temperature trends in North China. J. Clim. 21, 1333–1348.
Rizwan, A.M., Dennis, L.Y.C., Liu, C., 2008. A review on the generation, determination and mitigation of urban heat island. J. Environ. Sci. 20, 120–128.

Santamouris, M., Paraponiaris, K., Mihalakakou, G., 2007. Estimating the ecological footprint of the heat island effect over Athens, Greece. Clim. Chang. 80, 265–276.
Seto, K.C., Guneralp, B., Hutyra, L.R., 2012. Global forecasts of urban expansion to 2030 and direct impacts on biodiversity and carbon pools. Proc. Natl. Acad. Sci. U. S. A. 109, 16083–16088.
Sobstyl, J.M., Emig, T., Qomi, M.J.A., Ulm, F.J., Pellenq, R.J., 2018. Role of city texture in urban heat islands at nighttime. Phys. Rev. Lett. 120, 108701.
Streutker, D.R., 2002. A remote sensing study of the urban heat island of Houston, Texas. Int. J. Remote Sens. 23, 2595–2608.
Streutker, D., 2003. Satellite-measured growth of the urban heat island of Houston, Texas. Remote Sens. Environ. 85, 282–289.
Sun, Y., Gao, C., Li, J., Li, W., Ma, R., 2018. Examining urban thermal environment dynamics and relations to biophysical composition and configuration and socio-economic factors: a case study of the Shanghai metropolitan region. Sustain. Cities Soc. 40, 284–295.
Thompson, J.A., Paull, D.J., 2017. Assessing spatial and temporal patterns in land surface phenology for the Australian Alps (2000–2014). Remote Sens. Environ. 199, 1–13.
Tran, H., Uchihama, D., Ochi, S., Yasuoka, Y., 2006. Assessment with satellite data of the urban heat island effects in Asian mega cities. Int. J. Appl. Earth Obs. Geoinf. 8, 34–48.
Vargo, J., Stone, B., Habeeb, D., Liu, P., Russell, A., 2016. The social and spatial distribution of temperature-related health impacts from urban heat island reduction policies. Environ. Sci. Pol. 66, 366–374.
Wan, Z., 2008. New refinements and validation of the MODIS land-surface temperature/emissivity products. Remote Sens. Environ. 112, 59–74.
Yang, Q., Huang, X., Li, J., 2017. Assessing the relationship between surface urban heat islands and landscape patterns across climatic zones in China. Sci. Rep. 7, 9337–9347.
Yao, R., Wang, L., Huang, X., Guo, X., Niu, Z., Liu, H., 2017. Investigation of urbanization effects on land surface phenology in Northeast China during 2001–2015. Remote Sens. 9, 66–81.
Yao, R., Wang, L., Huang, X., Zhang, W., Li, J., Niu, Z., 2018. Interannual variations in surface urban heat island intensity and associated drivers in China. J. Environ. Manag. 222, 86–94.
Zhang, P., Imhoff, M.L., Wolfe, R.E., Bounoua, L., 2014. Characterizing urban heat islands of global settlements using MODIS and nighttime lights products. Can. J. Remote. Sens. 36, 185–196.
Zhao, L., Lee, X., Smith, R.B., Oleson, K., 2014. Strong contributions of local background climate to urban heat islands. Nature 511, 216–219.
Zhao, S., Zhou, D., Liu, S., 2016. Data concurrency is required for estimating urban heat island intensity. Environ. Pollut. 208, 118–124.
Zhou, D., Zhao, S., Liu, S., Zhang, L., Zhu, C., 2014. Surface urban heat island in China's 32 major cities: spatial patterns and drivers. Remote Sens. Environ. 152, 51–61.
Zhou, D., Zhao, S., Zhang, L., Sun, G., Liu, Y., 2015. The footprint of urban heat island effect in China. Sci. Rep. 5, 11160–11170.
Zhou, D., Zhang, L., Hao, L., Sun, G., Liu, Y., Zhu, C., 2016. Spatiotemporal trends of urban heat island effect along the urban development intensity gradient in China. Sci. Total Environ. 544, 617–626.
Zhou, B., Rybski, D., Kropp, J.P., 2017. The role of city size and urban form in the surface urban heat island. Sci. Rep. 7, 4791–4799.
Zhou, D., Bonafoni, S., Zhang, L., Wang, R., 2018. Remote sensing of the urban heat island effect in a highly populated urban agglomeration area in East China. Sci. Total Environ. 628, 415–429.